JOURNAL OF CATALYSIS 145, 312–317 (1994)

Conductivity and Phase Diagram of the SO_2 Oxidation Catalyst Model System: $M_2S_2O_7$–V_2O_5 (M = 80% K + 20% Na)

D. A. Karydis,* S. Boghosian,*,[1] and R. Fehrmann†

*Institute of Chemical Engineering and High Temperature Chemical Processes, and Department of Chemical Engineering, University of Patras, GR-26500 Patras, Greece; and †Chemistry Department A, The Technical University of Denmark, DK-2800 Lyngby, Denmark

Received April 15, 1993; revised July 20, 1993

The specific conductivities of the sulfuric acid catalyst model system $M_2S_2O_7$–V_2O_5 (M = 80% K + 20% Na) were measured at 14 different compositions in the range $\chi_{V_2O_5}$ = 0–0.3500 and in the temperature range 250–500°C. The phase diagram of the $M_2S_2O_7$–V_2O_5 (M = 80% K + 20% Na) system was constructed by estimating the liquidus and the solidus temperatures for each composition from the marked change of the conductivity at the phase transition temperatures. The melting point of the pyrosulfate mixture $K_2S_2O_7$–$Na_2S_2O_7$ (80%–20%) was found to be 378°C. Two eutectics were found at $\chi_{V_2O_5}$ = 0.175 and $\chi_{V_2O_5}$ = 0.30 with temperatures of fusion of 314 and 326°C, respectively. The local maximum exhibited in phase diagram at $\chi_{V_2O_5}$ = 0.25 and t = 338°C probably corresponds to the formation of the mixed cation compound $M_3VO_2SO_4S_2O_7$ (M = 80% K + 20% Na). The data indicate that the lowest temperature of operation for a widely used potassium and sodium promoted vanadium oxide based common sulfuric acid catalyst (VK 38, Haldor Topsøe A/S) in the oxidized form is 323°C. The results are considered to be of significance for the design of new low-temperature molten salt catalysts for SO_2 oxidation and flue gas desulfurization.

INTRODUCTION

The characterization of molten salt mixtures related to the sulfuric acid catalyst is considered to be the methodical way for understanding the catalyst's performance and for providing the basis for catalyst improvements. The industrial catalyst for oxidation of SO_2 to SO_3—the key step in the sulfuric acid production and in the flue gas desulfhurization—is a supported liquid phase (SLP) catalyst. It consists of a molten salt mixture of vanadium pentoxide and alkali pyrosulfates dispersed on an inert support (1). The liquid–gas system $M_2S_2O_7/V_2O_5$–$SO_2/O_2/SO_3/N_2$, where M is a mixture of about 80% K and 20% Na, describes well the active part of widely used commercial sulfuric acid catalysts, e.g., VK 38 from Haldor Topsøe A/S, Denmark.

The catalytic oxidation of SO_2 to SO_3 takes place as a homogeneous reaction in the liquid phase of the catalyst in the temperature range 420–600°C. At lower temperatures the catalyst deactivates. It was for a long time assumed that the deactivation was due to the precipitation of vanadium (IV) compounds (1–3). Recently, it was shown by investigating catalytic activity and compound formation in unsupported $M_2S_2O_7$–V_2O_5 (M = Na, K, Cs) molten salt systems (4) that crystalline vanadium (IV) and (III) compounds indeed are formed in these melts during SO_2 oxidation at the temperature where the deactivation starts. It was also shown (4) that the temperature of precipitation decreases as (i) the atomic number of the alkali promoter increases, (ii) the alkali-to-vanadium ratio increases, (iii) the SO_3/SO_2 ratio increases, and (iv) more of the alkali promoters are mixed. Furthermore, *in situ* ESR investigations of the catalyst VK 38 (5) also confirmed that the vanadium (IV) compound, $K_4(VO)_3(SO_4)_5$ (4), indeed is formed during catalyst deactivation.

The ultimate goal of research in this field is the development of a catalyst which will be active at temperatures below ca. 420°C, where the existing catalysts start to deactivate. The limiting temperature for the catalyst activity might be the liquidus temperature for the particular $M_2S_2O_7$–V_2O_5 mixture that corresponds to the oxidized form of the catalyst melt, i.e., at low partial pressure of SO_2 characteristic for the last bed of industrial converters. Knowledge of the phase diagrams for the $M_2S_2O_7$–V_2O_5 systems is therefore considered essential for the design of new low-temperature catalysts.

Several studies (6–9) of the phase diagram of the V_2O_5–$K_2S_2O_7$ binary system show marked discrepancies. This is demonstrated by the variation in the values published for the liquidus temperature at $\chi_{V_2O_5}$ = 0.5, namely, 590 (6), 490 (8), and 430°C (9). Also the composition of the eutectic is very uncertain and values of 92 (6), 85 (7), 90 (8), and 78 (9) mol% $K_2S_2O_7$ have been proposed. The large descrepancy is believed to have been caused either by the use of impure $K_2S_2O_7$ (contaminated by $KHSO_4$, as mentioned earlier (10)) or because of use of open cell

[1] To whom correspondence should be addressed.

0021-9517/94 $5.00

measuring systems giving rise to decomposition due to evaporation or reactions with atmospheric moisture.

Thus, reliable fundamental data such as the conductivity as well as the phase diagram of the $M_2S_2O_7$–V_2O_5 (M = 80% K + 20% Na) molten salt system are not available in the literature. The aim of the present study was to construct the phase diagram of this system from conductivity measurements, one of the few applicable useful methods for the high-temperature study of these hygroscopic, viscous, and very dark melts. A similar study has recently been carried out on the $Cs_2S_2O_7$–V_2O_5 system (11), where a maximum was found at $\chi_{V_2O_5} = 0.33$ in the phase diagram corresponding to the formation of a dimeric V(V) compound. This compound has been shown to be $Cs_4(VO)_2O(SO_4)_4$ (12).

EXPERIMENTAL

Chemicals

Pure and dry $K_2S_2O_7$ and $Na_2S_2O_7$ were obtained by thermal decomposition of the corresponding peroxodisulfates (10), $K_2S_2O_8$ was from Merck, Pro Analysi, and $Na_2S_2O_8$ was from Fluka, Pro Analysi. The purity of the molten pyrosulfates was checked by Raman spectroscopy as described previously (4). The nonhygroscopic V_2O_5 (Cerac, Pure 99.9%) was used without further purification. All handling of chemicals took place in a nitrogen filled glovebox with a water vapor content of about 5 ppm achieved by continuous recirculation through external molecular sieves. The pyrosulfates were kept in sealed ampules and opened only in the dry atmosphere of the glovebox.

Conductivity Measurements

For measuring the conductivity a borosilicate glass cell was used. It consists of two compartments connected through a capillary tube and a neck with a standard taper joint on top for the addition of the materials. A gold electrode is sealed vacuum tight into each compartment. Gold is apparently the only metal resistant to the melt. The conductivity cell has been described in detail elsewhere (13).

The cell was filled with chemicals in the glovebox and thereafter it was evacuated and closed by sealing the stem. After a composition was measured the stem was cut open in the glovebox and the composition was varied by addition of chemicals through the taper joint. The cell was then resealed before it was placed inside a metal block furnace regulated to within ±0.1°C. The furnace and its regulation has been described previously (14). The temperature of the melt was measured by a controlled chromel-alumel thermocouple or by a Pt-100 platinum resistance thermometer placed directly at the capillary tube.

The resistance between the electrodes was measured with a precision better than 0.1% by using a Wheatstone bridge at 2 kHz as described earlier (15), or by using a Radiometer CDM-83 conductivity meter. The cell constant, k, was determined in a thermostat at room temperature by measuring the resistance of a standard solution of known conductivity (13). Values from 100 up to 220 cm^{-1} were obtained as cell constants. Finally the conductivity, κ, is calculated from the equation $\kappa = k/R$, where R is the measured resistance of the melt. For each composition the conductivity was measured as a function of temperature in the range 250–480°C. The temperature was reduced in steps of 10 or 20°C down to the lowest measuring temperature, and the resistance was measured each time until it was larger than 10^6 Ω due to crystallization. The temperature was then raised in steps of 1–5°C in order to detect a possible subcooled state of the melt. By increasing the temperature both the crystallized and the liquid + solid region were investigated. Sometimes it was very difficult for the subcooled melt to crystallize—it took several days—especially for melts with a high content of V_2O_5 (i.e., $\chi_{V_2O_5} > 0.20$). The optimum temperature for crystallization of the subcooled melt was in the range 280–310°C depending on the composition, $\chi_{V_2O_5}$.

METHOD

The conductivity of ionic melts is related exponentially to the temperature

$$\kappa = A_\kappa e^{-E_\kappa/RT}$$

where κ is the conductivity, A_κ is a constant, E_κ is the energy necessary for the ionic migration, the so-called activation energy, R is the gas constant, and T is the absolute temperature. A plot of ln κ vs $1/T$ is usually a straight line in a limited temperature range and the slope is proportional to the activation energy, E_κ. When the phase changes from the liquid to the solid state, the activation energy is expected to change and a different slope is obtained. In the intermediate liquid + solid region the dependence of ln κ vs $1/T$ will deviate from these lines since the composition of the melt changes. Break points on the ln κ vs $1/T$ plots will therefore indicate phase-transition temperatures.

Contrary to the case of open cell measuring systems where sample decomposition due to evaporation and contamination due to reactions with atmospheric moisture are often encountered, the technique used in the present investigation permits the high-temperature study of viscous, hygroscopic, and deeply colored melts by avoiding such difficulties.

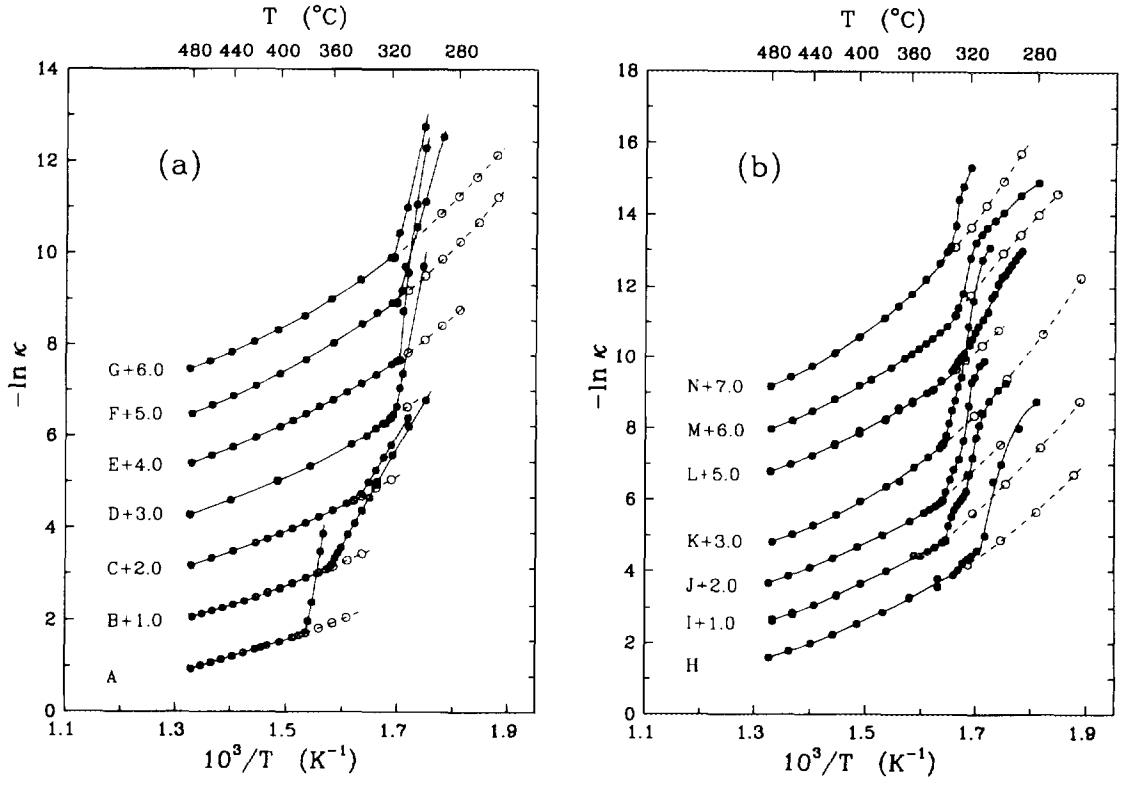

FIG. 1. Phase transitions in the $M_2S_2O_7$–V_2O_5 (M = 80% K and 20% Na) system, $-\ln \kappa$ vs $1/T$. (a) $\chi_{V_2O_5}$: (A) 0.0000, (B) 0.0500, (C) 0.1000, (D) 0.1500, (E) 0.1748, (F) 0.1873, and (G) 0.2000. (b) $\chi_{V_2O_5}$: (H) 0.2250, (I) 0.2398, (J) 0.2500, (K) 0.2697, (L) 0.2873, (M) 0.3000, and (N) 0.3501. For clarity, the data (except for those in plots A and H) are offset on the ordinate by the specified values. Open circles indicate subcooling.

RESULTS AND DISCUSSION

The specific conductivity of the $M_2S_2O_7$–V_2O_5 (M = 80% K + 20% Na) binary molten salt system has been measured at 14 different compositions in the mole fraction range $\chi_{V_2O_5}$ = 0–0.3500 and in the temperature range 250–480°C. The results of the measurements are shown in Fig. 1 where the specific conductivity κ is plotted as $-\ln \kappa$ vs $1/T$. There are three branches in the $\ln \kappa$ vs $1/T$ plot, representing liquid, liquid + solid, and solid state of the mixture in the cell. For some compositions only two branches for the liquid and the liquid + solid state were observed because the conductivity of the solid crystallized state was undetectably small.

For all compositions a weakly curved plot was found in the high-temperature region—the liquid phase of the system. For the solid phase a sharp almost vertical line was found in most of the experiments. Table 1 summarizes the phase-transition temperatures defined from the break points observed in Fig. 1.

The subcooled states are shown with open circles in Fig. 1. The subcooled melts were stable at low temperatures—in one case (F) down to 225°C—until the crystallization started, followed by a jump in the conductivity to lower values.

As previously (13, 16) empirical polynomia of the type $\kappa = A(\chi) + B(\chi)(t - 450) + C(\chi)(t - 450)^2 + D(\chi)(t - 450)^3$ have been fitted to the experimental data of the liquid region at each composition, $\chi_{V_2O_5}$, as presented in Table 2. Furthermore, for general use, an empirical equation for the conductivity of the form

$$\kappa = \sum_0^n A_n\chi^n + \sum_1^m B_m(t - 450)^m + \sum_1^l C_l\chi^l(t - 450)$$

has been calculated from the measured conductivities in the entire temperature and composition range of the liquid. The most satisfactory equation was found to be for $n = 2$, $m = 2$, and $l = 1$, and is expressed as

$$\kappa = 0.32548 - 0.8525\chi + 0.4127\chi^2 + 2.385 \times 10^{-3}(t - 450) + 4.284 \times 10^{-6}(t - 450)^2 - 3.361 \times 10^{-3}\chi(t - 450)$$

(SD = 0.00444 Ω^{-1} cm^{-1}) for $0 < \chi_{V_2O_5} < 0.3500$.

TABLE 1

Phase-Transition Temperatures for the $M_2S_2O_7$–V_2O_5 System (M = 80% K + 20% Na)

	Mole fraction $\chi_{V_2O_5}$	Liquidus point t (°C)	Solidus point t (°C)
A	0.0000	378.0	—
B	0.0500	362.0	—
C	0.1000	342.0	—
D	0.1500	322.0	316.0
E	0.1748	314.0	314.0
F	0.1873	316.0	—
G	0.2000	319.0	—
H	0.2250	328.0	315.0
I	0.2398	335.0	321.0
J	0.2500	338.0	326.0
K	0.2697	336.0	325.0
L	0.2873	331.0	—
M	0.3000	329.0	—
N	0.3501	342.0	331.5

Figure 2 shows the conductivity data plotted vs. the composition of the mixture, $\chi_{V_2O_5}$, for three different temperatures, 400, 440, and 480°C. It appears that (i) as expected, the conductivity decreases with decreasing temperature and (ii) it decreases with increasing amount of V_2O_5 added to the melt since V_2O_5 in the extrapolated liquid state has a very low conductivity (0.000435 and 0.002443 Ω^{-1} cm^{-1} at 400 and 480°C, respectively (17)).

Figure 3 shows the conductivity isotherms at 480°C of the $Cs_2S_2O_7$–V_2O_5 (16), $K_2S_2O_7$–V_2O_5 (13), and $M_2S_2O_7$–V_2O_5 (M = 80% K + 20% Na) molten mixtures. The highest conductivity among melts with $\chi_{V_2O_5}$ = 0 is

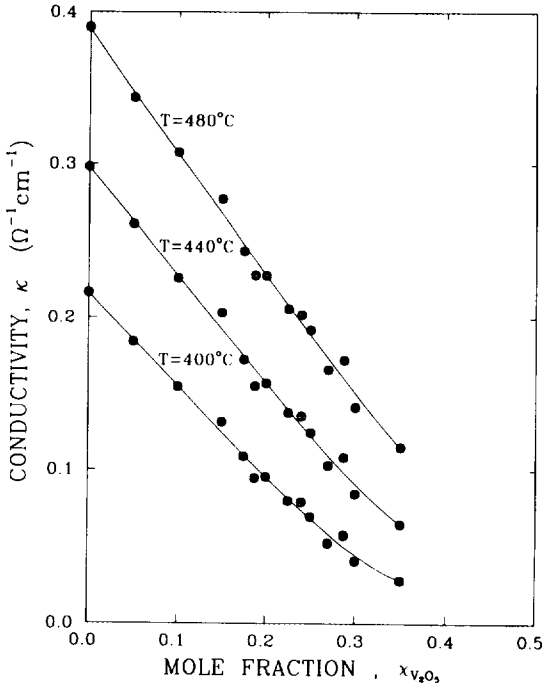

FIG. 2. Conductivity isotherms for the molten $M_2S_2O_7$–V_2O_5 (M = 80% K + 20% Na) system.

TABLE 2

Coefficients of the Empirical Equation $\kappa = A(\chi) + B(\chi)(t - 450) + C(\chi)(t - 450)^2 + D(\chi)(t - 450)^3$ for Different Compositions, $\chi_{V_2O_5}$, of the $M_2S_2O_7$–V_2O_5 (M = 80% K + 20% Na) System

$\chi_{V_2O_5}$	$A(\chi)$ (Ω^{-1} cm^{-1})	$10^3\ B(\chi)$ (Ω^{-1} cm^{-1} deg^{-1})	$10^6\ C(\chi)$ (Ω^{-1} cm^{-1} deg^{-2})	$10^9\ D(\chi)$ (Ω^{-1} cm^{-1} deg^{-3})	SD[a] (Ω^{-1} cm^{-1})
0.0000	0.32106	2.203	4.241	21.347	0.00092
0.0500	0.28401	2.067	1.980	−6.797	0.00034
0.1000	0.24820	2.024	3.391	−1.684	0.00098
0.1500	0.21917	1.879	2.308	−9.467	0.00119
0.1748	0.19228	1.782	3.033	−7.776	0.00054
0.1873	0.17336	1.759	3.790	−4.968	0.00072
0.2000	0.17520	1.745	2.900	−10.433	0.00011
0.2250	0.15304	1.663	2.834	−15.661	0.00180
0.2398	0.14777	1.693	3.764	−13.129	0.00428
0.2500	0.13844	1.606	4.263	−5.785	0.00049
0.2697	0.11948	1.525	4.776	−1.824	0.00101
0.2873	0.12341	1.551	4.432	−6.031	0.00151
0.3000	0.09809	1.358	5.222	−1.827	0.00089
0.3501	0.07652	1.185	4.734	−0.270	0.00043

[a] Standard deviation.

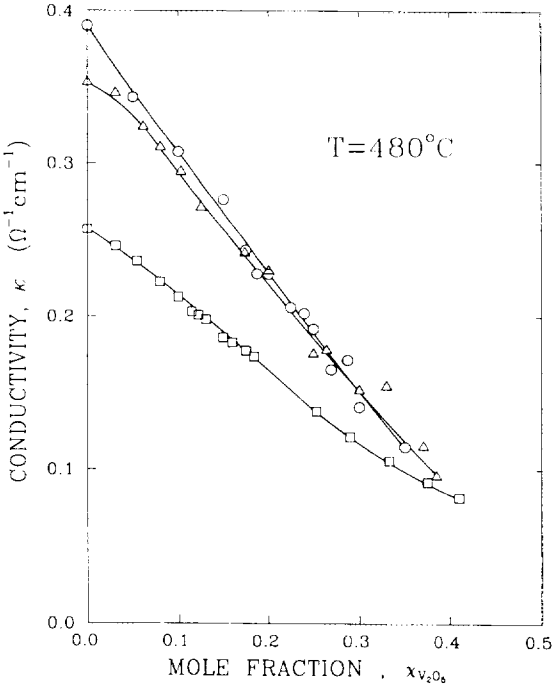

FIG. 3. Conductivity isotherms at 480°C for the molten systems $M_2S_2O_7$–V_2O_5 (M = Cs, □ (16); K, △ (13); and 80% K + 20% Na, ○ (this work)).

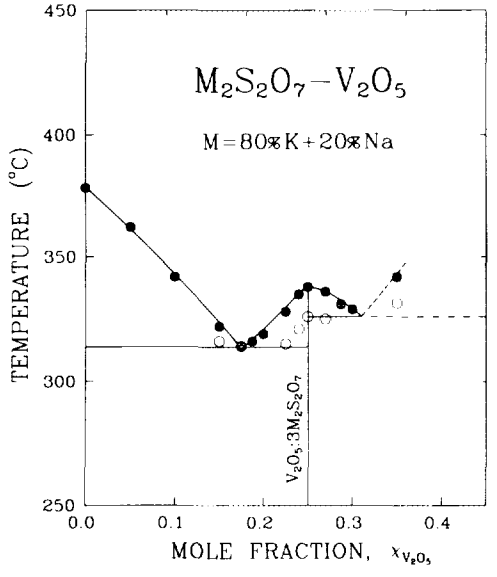

FIG. 4. Phase diagram of the $M_2S_2O_7$–V_2O_5 (M = 80% K + 20% Na) system.

seen for the (K + Na)$_2S_2O_7$ mixture. Apparently the conductivity decreases in the sequence $Na_2S_2O_7$, $K_2S_2O_7$, $Cs_2S_2O_7$. As the mobility (and hereby the conductivity) decreases with increasing ionic radius this finding supports the assumption that M^+ is the main current carrier. With increasing amounts of V_2O_5 in the melt, the conductivities become more and more similar. Above $\chi_{V_2O_5}$ = 0.15, the conductivity of the sodium-containing mixtures is practically identical to that of the potassium melts, and on going to $\chi_{V_2O_5}$ = 0.40, the conductivities of the potassium and cesium melts coincide. This could be an indication that the melts become more and more alike, i.e., the same types of conducting complexes are formed in the various systems.

Figure 4 shows the phase diagram for the $M_2S_2O_7$–V_2O_5 (M = 80% K + 20% Na) binary molten salt system, which is constructed from the marked change in the conductivity at the phase transition temperatures (see Method section). At mole fractions, $\chi_{V_2O_5}$, higher than around 0.4, phase transitions could not be observed, possibly due to the pronounced tendency for glass formation without crystallization in this V_2O_5-rich composition range of the pseudobinary system. Most probably, the phase diagram is completed by a line extrapolating to 670°C—the temperature of fusion of V_2O_5. The temperature of fusion of the $K_2S_2O_7$–$Na_2S_2O_7$ (80% K + 20% Na) mixture was found to be 378°C which—as expected—is lower than both the melting point of $K_2S_2O_7$ (419°C (18)) and of $Na_2S_2O_7$ (404°C (19)). Two eutectics are found at $\chi_{V_2O_5}$ = 0.175 and $\chi_{V_2O_5}$ = 0.30 with temperatures of fusion of 314 and 326°C, respectively. It should be noted that—as expected—the temperature regime between the two breakpoints of a $-\ln\kappa$ vs $1/T$ plot (Fig. 1), i.e., the liquidus and the temperature of fusion of the eutectic, where a mixture of solid and liquid is present, becomes increasingly smaller as the composition approaches a eutectic. Therefore, only one break is observed in plots F, G, L, and M corresponding to the liquidus temperature (see also Table 1). A maximum in the phase diagram is found at $\chi_{V_2O_5}$ = 0.25 and with a liquidus temperature 338°C—probably due to the formation of a compound with the stoichiometry $3M_2S_2O_7 : 1V_2O_5$ (M = 80% K + 20% Na). A compound corresponding to this composition with the proposed formula $K_3VO_2SO_4S_2O_7$ has earlier (20) been isolated from the $K_2S_2O_7$–V_2O_5 system. If this compound—containing only K—was formed also in the present pseudobinary $M_2S_2O_7$–V_2O_5 (M = 80% K + 20% Na) system, it should have been formed to a maximum extent at $\chi_{V_2O_5}$ = 0.21. Indeed a peritectic might be present at this composition in the phase diagram (Fig. 4), but more measurements are needed for confirmation. Surprisingly, there is no sign of formation of dimeric vanadium (V) compounds in this system, since no maxima are found at $\chi_{V_2O_5}$ = 0.33 or $\chi_{V_2O_5}$ = 0.29 corresponding to the compositions $2M_2S_2O_7 : 1V_2O_5$ and $2K_2S_2O_7 : 1V_2O_5$, respectively. In the phase diagrams of the analogous $Cs_2S_2O_7$–V_2O_5 and $K_2S_2O_7$–V_2O_5 systems, a local maximum is found at this composition (11, 21) and a dimeric compound, $Cs_4(VO)_2O(SO_4)_4$, has recently been isolated and characterized (11, 12). Attempts to isolate possible vanadium (V) compounds from the pseudobinary $M_2S_2O_7$–V_2O_5 (M = 80% K + 20% Na) molten system by cooling in an ampoule failed. However, the V(IV)–V(V) mixed valence compound $K_6(VO)_4(SO_4)_8$, described elsewhere (22), was found besides an amorphous phase that most probably contained vanadium (V).

It is well established that in dilute (18) as well as in more concentrated (13, 23) solutions of vanadium pentoxide in alkali pyrosulfate melts, V_2O_5 probably transforms to vanadium (V) complexes of the so-called oxosulfatovanadate type. Isolation of the potassium and cesium oxosulfatovanadates KVO_2SO_4, $K_4(VO_2)_2(SO_4)_2S_2O_7$, and $K_3VO_2SO_4S_2O_7$ (20), and $Cs_4(VO)_2O(SO_4)_4$ (11, 12) supports the above statement. Furthermore, the formation of trivalent and tetravalent vanadium compounds $NaV(SO_4)_2$, $Na_2VO(SO_4)_2$, $KV(SO_4)_2$, $K_4(VO)_3(SO_4)_5$, $CsV(SO_4)_2$, and $Cs_2(VO)_2(SO_4)_3$, *during* SO_2 oxidation in $M_2S_2O_7$–V_2O_5 (M = Na, K, and Cs) melts (4), points to the existence of vanadium–oxosulfato complexes in solution.

A reaction accounting for the formation of a vanadium (V) complex with the stoichiometry $3M_2S_2O_7 : 1V_2O_5$ mentioned above is (18)

$$V_2O_5 + 3S_2O_7^{2-} \rightarrow 2VO_2SO_4S_2O_7^{3-}.$$

CONCLUSIONS

The phase diagram of the $M_2S_2O_7$–V_2O_5 (M = 80% K + 20% Na) system has been constructed. Two eutectics were found at $\chi_{V_2O_5} = 0.175$ and $\chi_{V_2O_5} = 0.30$ with temperatures of fusion of 314 and 326°C, respectively. The molten phase of the widely used Haldor Topsøe VK38 commercial catalyst consisted of vanadium pentoxide–alkali pyrosulfate mixture has a composition reflected by the ratio K : Na : V = 3 : 0.8 : 1. Therefore, the molten system $M_2S_2O_7$–V_2O_5 (M = 80% K + 20% Na) with composition $\chi_{V_2O_5} = 0.21$ is most probably a realistic model of the molten catalyst in its oxidized form, i.e., as found in the last bed of an industrial catalytic converter, where due to the low SO_2 and high SO_3 partial pressures the redox equilibria involving vanadium complexes are shifted to the V(V) side (24). Thus the lowest operating temperature of the molten salt catalyst in its oxidized form seems to be around 323°C—the liquidus temperature of the $M_2S_2O_7$–V_2O_5 (80% K + 20% Na) mixture with $\chi_{V_2O_5} = 0.21$. This result is of significance for achieving the long-sought goal of a low-temperature sulfuric acid catalyst and for designing new catalysts for flue gas desulfurization.

ACKNOWLEDGMENTS

This investigation has been supported by the EEC BRITE-EURAMII Project BRE2.CT93.0447 and the Danish Natural Science Research Council. Keld W. Petersen is gratefully acknowledged for experimental assistance. The authors thank N. J. Bjerrum and G. N. Papatheodorou for helpful discussions and valuable comments.

REFERENCES

1. Villadsen, J., and Livbjerg, H., *Catal. Rev.-Sci. Eng.* **17,** 103 (1978).
2. Doering, F., and Bercel, D., *J. Catal.* **103,** 126 (1987).
3. Borescov, G. K., Polyakova, G. M., Ivanov, A. A., and Mastikhin, V. M., *Dokl. Akad. Nauk. SSSR* **210,** 626 (1973).
4. Boghosian, S., Fehrmann, R., Bjerrum, N. J., and Papatheodorou, G. N., *J. Catal.* **119,** 121 (1989).
5. Eriksen, K. M., Fehrmann, R., and Bjerrum, N. J., *J. Catal.* **132,** 263 (1991).
6. Bazarova, Zh. G., Boreskov, G. K., Kefeli, L. M., Karakchiev, L. G., and Ostankowich, A. A., *Dokl. Akad. Nauk SSSR* **180,** 1132 (1968).
7. Hähle, S., and Meisel, A., *Kinet. Katal.* **12,** 1276 (1971).
8. Maslennikov, B. M., Illarionov, V. V., Gubareva, V. N., Bushuev, N. N., Tavrovskaya, A. Ya., and Leneva, Z. L. *Dokl. Acad. Nauk. SSSR* **238,** 1411 (1978).
9. Glazyrin, M. P., Krasil'nikov, V. N., and Ivakin, A. A., *Zh. Neorg. Khim.* **25,** 3368 (1980).
10. Fehrmann, R., Hansen, N. H., and Bjerrum, N. J., *Inorg. Chem.* **22,** 4009 (1983).
11. Folkmann, G. E., Hatem, G., Fehrmann, R., Gaune-Escard, M., and Bjerrum, N. J., *Inorg. Chem.* **30,** 4057 (1991).
12. Niesen, K., Fehrmann, R., and Eriksen, K. M., *Inorg. Chem.* **32,** in press (1993).
13. Hatem, G., Fehrmann, R., Gaune-Escard, M., and Bjerrum, N. J., *J. Phys. Chem.* **91,** 195 (1987).
14. Andreasen, H. A., Bjerrum, N. J., and Forerskov, C. E., *Rev. Sci. Instrum.* **48,** 1340 (1977).
15. Poulsen, F. W., and Bjerrum, N. J., *J. Phys. Chem.* **79,** 1610 (1975).
16. Folkmann, G. E., Hatem, G., Fehrmann, R., Gaune-Escard, M., and Bjerrum, N. J., *Inorg. Chem.* **32,** 1559 (1993).
17. Pantony, D. A., and Vasu, K. I., *J. Inorg. Nucl. Chem.* **30,** 433 (1968).
18. Hansen, N. H., Fehrmann, R., and Bjerrum N. J., *Inorg. Chem.* **21,** 744 (1982).
19. Krasil'nikov, V. N., Glazyrin, M. P., Palkin, A. P., Perelyaeva, L. A. and Ivakin, A. A., *Russ. J. Inorg. Chem. (Engl. Transl.)* **25,** 1843 (1980).
20. Glazyrin, M. P., Krasil'nikov, V. N., and Ivakin, A. A., *Russ. J. Inorg. Chem. (Engl. Transl.)* **32,** 425 (1987).
21. Bandur, V. A., Eriksen, K. M., Folkmann, G. E., Hatem, G., Fehrmann, R., and Bjerrum N. J., in preparation.
22. Eriksen, K. M., Nielsen, K., and Fehrmann, R., in preparation.
23. Fehrmann R., Gaune-Escard, M., and Bjerrum N.J., *Inorg. Chem.* **25,** 1132 (1986).
24. Karydis, D. A., Eriksen, K. M., Fehrmann, R. and Boghosian, S., in preparation.